Electron-impact excitation cross sections of the higher argon $3p^5np$ $(n=5,6,7)$ levels

Tobin Weber, John B. Boffard, and Chun C. Lin
Department of Physics, University of Wisconsin, Madison, Wisconsin 53706, USA
(Received 19 May 2003; published 23 September 2003)

We have measured the electron-impact excitation cross sections for argon into the ten levels of $3p^5 5p$ configuration, as well as numerous levels of the $3p^5 6p$ and $3p^5 7p$ configurations. Fluorescence from the decay of the excited atoms to the levels of $3p^5 4s$ configuration was used to determine the optical-emission cross sections. These results were combined with transition probabilities to find apparent cross sections into the $3p^5 5p$ and $3p^5 6p$ levels. These new cross sections of the Ar$(3p^5 np)$ levels along with the available Ne$(2p^5 3p)$, Kr$(4p^5 5p)$, and Xe$(5p^5 6p)$ data help provide a global view of the excitation behaviors of the $np^5 n'p$ levels of the rare-gas series.

DOI: 10.1103/PhysRevA.68.032719 PACS number(s): 34.80.My, 34.80.Dp

I. INTRODUCTION

The visible spectrum of an argon discharge is dominated by the emissions from the levels of the $3p^5 4p$ configuration ($2p$ in Paschen's notation) for red/near-ir wavelengths and from the $3p^5 5p$ levels ($3p$ in Paschen's notation) for blue wavelengths. Under most plasma conditions, the primary population mechanism for these levels is electron-impact excitations. Cross sections for excitation into the $3p^5 4p$ levels have been studied by many research groups [1,2], however, excitation into the $3p^5 5p$ levels have been less well studied [2–5]. This lack of recent reliable measurements is a hindrance to the use of these levels in some plasma diagnostic applications [6,7]. The $3p^5 5p \rightarrow 3p^5 4s$ ($3p \rightarrow 1s$) emissions lie in the same wavelength range as many intense argon-ion emission lines, making these neutral emissions relatively useful for plasma diagnostic experiments.

There are, however, some problems with measuring cross sections into the $3p$ levels. First, atoms in a $3p$ level can decay to levels in three lower-lying configurations (Paschen's designation in parentheses): the $3p^5 4s$ ($1s$), $3p^5 5s$ ($2s$), and $3p^5 3d$ ($3d$). While the $3p \rightarrow 1s$ emissions lie in a favorable region of the spectrum (300–500 nm, see Table I), the $3p \rightarrow 2s,3d$ emissions are in the infrared (1.4–7.7 μm) and generally much harder to detect. Transition probabilities indicate that only (5–35)% of atoms excited to $3p$ levels decay to the $1s$ levels [8]. Since all previous measurements have been limited to the $3p \rightarrow 1s$ transitions, it has been difficult to determine even the general magnitude of the apparent cross sections for these levels. The second difficulty is that even within the $3p \rightarrow 1s$ transition array there are many difficulties in measuring the emission lines [2,9]. We consider three simple examples: (i) all of the transitions out of the $3p_3$ level lie within 0.2 nm of a transition from the $3p_2$ level; (ii) the $3p_4 \rightarrow 1s_3$ and $3p_8 \rightarrow 1s_5$ transitions are both at 419.1 nm; and (iii) many weak transitions ($3p_1 \rightarrow 1s_4$, $3p_6 \rightarrow 1s_2$) lie within 0.2 nm of a strong argon-ion emission line. As a result, even within the $3p \rightarrow 1s$ transition array the emissions from all of the levels have rarely been measured.

In this paper we report optical-emission cross sections for the entire $3p \rightarrow 1s$ transition array ($3p^5 5p \rightarrow 3p^5 4s$ in configuration notation). Upon dividing the emission cross section for the $i \rightarrow j$ transition by the corresponding branching fraction one obtains the apparent excitation cross section of level i. In our previous experiments on excitation of the $2p$ levels ($3p^5 4p$), the branching fractions are determined by measuring the emission cross sections for all the transitions from the $2p$ levels. For the present work since the $3p \rightarrow 2s$ and $3p \rightarrow 3d$ emissions are in an unfavorable part of the spectrum as explained earlier, we obtain the $3p \rightarrow 1s$ branching fractions by combining the measured values of the $3p \rightarrow 1s$ transition probabilities and the $3p$ lifetimes in order to determine apparent excitation cross sections.

Another objective of this work is to study the excitation behaviors of the higher $3p^5 np$ configurations. We have measured optical-emission cross sections for selected $4p \rightarrow 1s$ and $5p \rightarrow 1s$ transitions ($3p^5 6p \rightarrow 3p^5 4s$ and $3p^5 7p \rightarrow 3p^5 4s$, respectively) and obtained the apparent excitation cross sections. In these configurations the outer electron (np) is far apart from the $3p^5$ core so that the interaction of the outer electron with the core is much weaker than the spin-orbit coupling of the $3p^5$ core. This situation is very much like the Xe atom (and Kr to a slightly less extent) where the spin orbit of the $5p^5$ core is so large that it overpowers the coupling of the $5p^5$ with the outer electron even for the lowest excited configurations. As will be seen, the cross sections for the Ar$(3p^5 np, n=5,6,7)$ bridge the cross-section behaviors observed in Ne$(2p^5 3p)$ and Ar$(3p^5 4p)$ with the very different behaviors for Kr$(4p^5 5p)$ and Xe$(5p^5 6p)$, and help provide a global understanding of the excitation cross sections from the standpoint of atomic structure especially the very intricate angular-momentum coupling in rare-gas atoms.

II. METHOD

The optical method for measuring cross sections is well known and detailed descriptions can be found elsewhere [10]. We limit our description here to defining the basic terms we use. The optical-emission cross section for the $i \rightarrow j$ transition at an electron energy E is defined to be

$$Q_{ij}^{opt}(E) \equiv \frac{\Phi_{ij}(E)}{n_0[I(E)/e]}, \tag{1}$$

TABLE I. Wavelengths of $3p \rightarrow 1s$ transitions in nanometer. Weak transitions (branching fraction less than 0.01) are marked with a subscript *w*. Transitions contaminated by an ion emission line have a subscript *i*. Transitions separated by less than 0.2 nm from another argon atom line are in italics. Dipole forbidden transitions are left blank.

	$3p_1$ $5p'[\frac{1}{2}]_0$	$3p_2$ $5p'[\frac{1}{2}]_1$	$3p_3$ $5p'[\frac{3}{2}]_2$	$3p_4$ $5p'[\frac{3}{2}]_1$	$3p_5$ $5p[\frac{1}{2}]_0$	$3p_6$ $5p[\frac{3}{2}]_2$	$3p_7$ $5p[\frac{3}{2}]_1$	$3p_8$ $5p[\frac{5}{2}]_2$	$3p_9$ $5p[\frac{5}{2}]_3$	$3p_{10}$ $5p[\frac{1}{2}]_1$
$1s_2$ $4s'[\frac{1}{2}]_0^o$	425.9	*433.5*	*433.4*	434.5	451.1	$458.9_{w,i}$	459.6_i	462.8_w		470.2
$1s_3$ $4s'[\frac{1}{2}]_1^o$		418.2		*419.1*			$442.4_{w,i}$			452.2
$1s_4$ $4s[\frac{3}{2}]_1^o$	$398.0_{w,i}$	*404.6*$_w$	*404.4*	$405.5_{w,i}$	419.8	426.6_i	427.2	430.0_i		$436.4_{w,i}$
$1s_5$ $4s[\frac{3}{2}]_2^o$		*394.9*	*394.8*$_w$	395.7_w		415.9	416.4	*419.1*	420.1	425.1

where Φ_{ij} is the number of photons per second per unit beam length at wavelength λ_{ij}, n_0 is the number density of target atoms (which is proportional to the gas pressure), I is the electron-beam current, and e is the charge of the electron. The sum of the optical-emission cross sections for all transitions out of level i is called the apparent excitation cross section,

$$Q_i^{app}(E) = \sum_{j<i} Q_{ij}^{opt}(E). \tag{2}$$

Conversely, any given optical-emission cross section can be found by multiplying the apparent cross section for level i by the branching fraction of the $i \rightarrow j$ transition,

$$Q_{ij}^{opt}(E) = Q_i^{app}(E) \frac{A_{ij}}{\sum_{k<i} A_{ik}}. \tag{3}$$

In the case of the Ar $3p$ levels, the transition probabilities of the $3p \rightarrow 1s$ transitions are known to reasonable accuracy (generally within $\pm 10\%$) [8,11]. While the individual transition probabilities of the $3p \rightarrow 2s,3d$ transitions are less well known, we take note that the sum of all transition probabilities out of a level is the inverse of the level's lifetime τ, which have been previously measured for the $3p$ levels [8,12–15]. Hence, we can obtain the apparent cross section for a $3p_x$ level from Eq. (3) by summing over the $3p_x \rightarrow 1s$ optical-emission cross sections and dividing by the branching fraction for the entire $3p_x \rightarrow 1s$ group of transitions,

$$Q_{3p_x}^{app}(E) = \sum_{1s_y} Q_{3p_x \rightarrow 1s_y}^{opt}(E) \frac{\sum_{k<3p_x} A_{3p_x \rightarrow k}}{\sum_{1s_y} A_{3p_x \rightarrow 1s_y}}. \tag{4}$$

In Table II we list the literature derived values for the $3p \rightarrow 1s$ transition probabilities needed for this work as tabulated from Ref. [8]. The required $3p$ lifetime values as derived from literature are also included in Table II. We have used two main criteria for selecting among the numerous, and sometimes conflicting (see Refs. [15,16]), lifetime measurements. Due to the strong collisional quenching [13], accurate extraction of the $3p$ radiative lifetimes require extrapolation to zero pressure. Hence, we prefer to use values obtained at low pressures (i.e., ones at or below the pressure used in this work: 6 mTorr). The second criterion is to prefer measurements in which the atoms in the $3p$ levels are produced by laser excitation rather than electron-impact excitation, since the laser excitation process is more selective and should thus eliminate the complications of cascades. Unfortunately, only two of the experiments simultaneously satisfy both criteria [8,15], and they are for the same $3p_8$ level. As a result we have generally averaged the results from different experiments weighing each by the relative experimental advantages offered for each level.

For the argon $4p$ and $5p$ levels both the transition probabilities and lifetimes have been much less studied. The $4p \rightarrow 1s$ transition probabilities are only known to about $\pm 30\%$ [17,18,14]. We have only found experimental measurements for eight of the ten $4p$ levels [14,19–21], the remaining two have been taken from theoretical calculations [22]. For the $5p \rightarrow 1s$ transitions we have found only two transition probabilities [17], but no lifetime measurements. Table III summarizes the transition probabilities for the $4p$ and $5p$ transitions observed in this work.

The apparent excitation cross section of level i includes the population of this level by direct electron-impact excita-

TABLE II. Transition probabilities and lifetimes of $3p$ levels derived from the literature.

Level	$\Sigma_{1s} A_{ij}$ (10^6 s^{-1}) [a]	$\tau_i^{-1} = \Sigma A_{ij}$ (10^6 s^{-1})
$3p_1$	3.98 ± 0.28	13.0 ± 1.7[b,c]
$3p_2$	1.44 ± 0.14	6.8 ± 1.4[c,d]
$3p_3$	0.96 ± 0.08	6.9 ± 1.2[c,d]
$3p_4$	0.86 ± 0.11	6.2 ± 0.8[c,d]
$3p_5$	3.75 ± 0.29	10.3 ± 1.0[b,c,d]
$3p_6$	1.72 ± 0.16	6.8 ± 1.6[b,c,d]
$3p_7$	1.19 ± 0.10	6.9 ± 1.0[b,c,d]
$3p_8$	0.70 ± 0.04	6.54 ± 0.07[a,e]
$3p_9$	0.97 ± 0.07	7.1 ± 0.8[b,c,d]
$3p_{10}$	0.32 ± 0.03	6.0 ± 0.9[b,c,d]

[a]Reference [8].
[b]Reference [12].
[c]Reference [14].
[d]Reference [13].
[e]Reference [15].

TABLE III. Data for $4p$ and $5p$ transitions observed in this work. Estimated uncertainties in A_{ij} values are $\pm 35\%$ (unless noted) based upon a comparison of independent measurements of Refs. [14,18]. Estimated uncertainties in experimentally measured lifetimes are taken as $\pm 10\%$ [inflated from quoted uncertainties of (2–5)%]. Uncertainty of theoretical lifetimes is estimated to $\pm 25\%$ based upon agreement between calculated values [22] and experimental measurements for remaining levels.

Transition	λ (nm)	A_{ij} (10^6 s^{-1})[a]	$\tau_i^{-1}=\sum A_{ij}$ (10^6 s^{-1})
$4p_1\rightarrow 1s_2$	365.0	0.80	5.3[b]
$4p_2\rightarrow 1s_2$	367.5	0.049	3.7[c]
$4p_3\rightarrow 1s_2$	367.1	0.031	3.9[c]
$\rightarrow 1s_4$	346.1	0.067	
$4p_4\rightarrow 1s_4$	356.3	0.12	3.8[d]
$4p_5\rightarrow 1s_2$	383.5	0.75	5.8[b,e]
$\rightarrow 1s_4$	360.7	0.76	
$4p_6\rightarrow 1s_4$	363.3	0.066	3.9[f]
$\rightarrow 1s_5$	355.4	0.27	
$4p_7\rightarrow 1s_4$	363.5	0.13	3.6[f]
$4p_8\rightarrow 1s_4$	364.3	0.024	3.8[f]
$4p_9\rightarrow 1s_5$	356.8	0.11	4.0[d]
$4p_{10}\rightarrow 1s_2$	389.5	0.057	3.1[b]
$\rightarrow 1s_4$	366.0	0.044	
$5p_1\rightarrow 1s_2$	340.6	0.39 ± 0.19	2.0[d]
$5p_5\rightarrow 1s_2$	357.2	0.51 ± 0.25	2.7[d]

[a]Reference [17].
[b]Reference [14].
[c]Reference [20].
[d]Reference [22] (theoretical).
[e]Reference [19].
[f]Reference [20].

tion and by cascades from electron-impact excitation into higher levels followed by radiative decay into the level *i*. The latter is equal to the sum of Q_{li}^{opt} over all levels (l) above level *i*. Thus the direct excitation cross section is obtained by making the ''cascade correction'' to the apparent cross section, i.e.,

TABLE V. Optical-emission cross sections for $3p^5 6p$ and $3p^5 7p$ ($4p$ and $5p$ in Paschen's notation) levels at 40 eV and 6 mTorr. Error bars include both the statistical and systematic uncertainties. Values for the apparent cross section were derived from Eq. (4) using transition probabilities listed in Table III. Uncertainty estimates for Q_i^{app} include the added uncertainties from transition probabilities.

$i\rightarrow j$ Transition	λ$_{ij}$ (nm)	Q_{ij}^{opt} (10^{-19} cm^2)	Q_i^{app} (10^{-19} cm^2)
$4p_1\ (J=0)\rightarrow 1s_2$	365.0	0.24 ± 0.03	1.6 ± 0.6
$4p_2\ (J=1)\rightarrow 1s_2$	367.5	0.013 ± 0.002	0.98 ± 0.37
$4p_3\ (J=2)\rightarrow 1s_2$	367.1	0.032 ± 0.009	2.7 ± 1.4
$\rightarrow 1s_4$	346.1	0.035 ± 0.007	
$4p_4\ (J=1)\rightarrow 1s_4$	356.3	0.019 ± 0.008	0.60 ± 0.26
$4p_5\ (J=0)\rightarrow 1s_2$	383.5	0.45 ± 0.03	3.5 ± 1.3
$\rightarrow 1s_4$	360.7	0.45 ± 0.03	
$4p_6\ (J=2)\rightarrow 1s_4$	363.3	0.034 ± 0.007	1.8 ± 0.6
$\rightarrow 1s_5$	355.4	0.12 ± 0.02	
$4p_7\ (J=1)\rightarrow 1s_4$	363.5	0.09 ± 0.02	2.5 ± 0.9
$4p_8\ (J=2)\rightarrow 1s_4$	364.3	0.025 ± 0.005	4.0 ± 1.5
$4p_9\ (J=3)\rightarrow 1s_5$	356.8	0.032 ± 0.006	1.2 ± 0.5
$4p_{10}(J=1)\rightarrow 1s_2$	389.5	0.019 ± 0.007	1.0 ± 0.4
$\rightarrow 1s_4$	366.0	0.016 ± 0.003	
$5p_1\ (J=0)\rightarrow 1s_2$	340.6	0.17 ± 0.05	0.87 ± 0.43
$5p_2\ (J=1)\rightarrow 1s_5$	317.3	0.017 ± 0.004	
$5p_5\ (J=0)\rightarrow 1s_2$	357.2	0.30 ± 0.05	1.6 ± 0.8
$5p_6\ (J=2)\rightarrow 1s_5$	331.9	0.045 ± 0.012	
$5p_9\ (J=3)\rightarrow 1s_5$	332.6	0.007 ± 0.002	

$$Q_i^{dir}(E)=Q_i^{app}(E)-\sum_{l>i} Q_{li}^{opt}. \qquad (5)$$

The apparatus used in this work is the same as that used in our earlier work to measure cross sections for the Ar $3p^5 4p$ levels [1]. The electron gun is located inside a 10-cm-diameter collision chamber which is evacuated to a base pressure of 2×10^{-8} Torr and then backfilled with 99.9995% purity argon gas. The gas pressure is measured with a spinning rotor gauge. The electron beam is formed from an indi-

TABLE IV. Optical emission cross sections in units of 10^{-19} cm^2 at 40 eV and 6 mTorr. Error bars include both the statistical and systematic uncertainties. Values for the apparent cross section were derived from Eq. (4) using transition probabilities listed in Table II. Uncertainty estimates for Q^{app} include the added uncertainties from transition probabilities.

	$3p_1$ ($J=0$)	$3p_2$ ($J=1$)	$3p_3$ ($J=2$)	$3p_4$ ($J=1$)	$3p_5$ ($J=0$)	$3p_6$ ($J=2$)	$3p_7$ ($J=1$)	$3p_8$ ($J=2$)	$3p_9$ ($J=3$)	$3p_{10}$ ($J=1$)
$1s_2$ ($J=1$)	2.41 ± 0.29	0.21 ± 0.04	0.36 ± 0.07	0.21 ± 0.03	1.00 ± 0.18	0.01 ± 0.01	0.11 ± 0.04	0.08 ± 0.03		0.13 ± 0.03
$1s_3$ ($J=0$)		0.33 ± 0.03		0.27 ± 0.07			0.02 ± 0.02			0.04 ± 0.02
$1s_4$ ($J=1$)	0.01 ± 0.01	0.02 ± 0.01	0.27 ± 0.06	0.015 ± 0.015	2.80 ± 0.38	0.29 ± 0.07	1.31 ± 0.18	0.88 ± 0.12		0.007 ± 0.005
$1s_5$ ($J=2$)		0.16 ± 0.03	0.06 ± 0.01	0.005 ± 0.005		1.45 ± 0.19	0.72 ± 0.12	0.46 ± 0.11	1.04 ± 0.15	0.09 ± 0.02
$\Sigma Q_{x\rightarrow 1s}^{opt}$	2.42	0.72	0.69	0.50	3.80	1.75	2.16	1.42	1.04	0.27
Q^{app} (6 mTorr)	7.9 ± 1.5	3.4 ± 1.1	5.0 ± 1.6	3.6 ± 1.1	10.4 ± 2.0	6.9 ± 2.0	12.5 ± 3.3	13.3 ± 2.5	7.6 ± 1.5	5.0 ± 1.7
Q^{app} (0 mTorr)	6.3 ± 1.2	2.4 ± 0.7	3.0 ± 1.3	3.1 ± 0.9	6.7 ± 1.3	6.0 ± 1.7	3.9 ± 1.4	11.5 ± 2.2	3.2 ± 0.8	2.7 ± 0.9

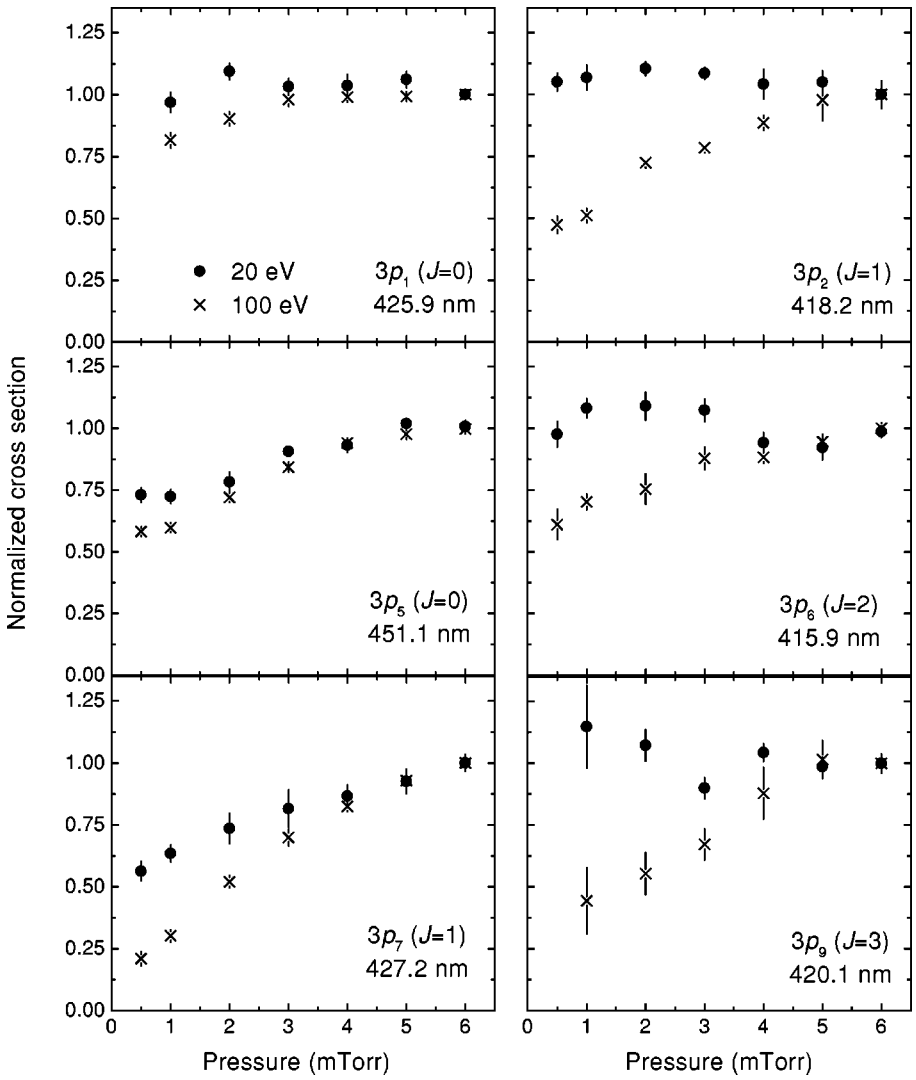

FIG. 1. Pressure dependence of optical-emission cross sections for selected $3p^5 5p$ levels.

rectly heated barium-oxide cathode and electrostatically focused by four grids before entering a deep Faraday cup used to collect the electron-beam current. Light from excited atoms emerges from a slit in the side of the Faraday cup and is imaged onto the entrance slit of a 1.26-m Czerny-Turner monochromator. The photons are recorded by a C31034A-02 photomultiplier tube. The output of the optical detection is placed on an absolute scale by the use of a tungsten-halogen standard lamp. The total systematic uncertainty in our optical-emission cross-section measurements is estimated to be $\pm 12\%$. As a general check of our data collection and analysis procedures, we have measured the He 4^1S (504.8 nm) and 5^1S (443.8 nm) optical-emission cross sections and compared them to the benchmark measurements of Van Zyl *et al.* [23]. All measurements agreed within error bars, with an average difference less than 10%.

We measured the polarization of the fluorescence by placing a polarizing filter between the collision chamber and the monochromator. The polarization dependence of the optical system was corrected for by ratioing the results to an unpolarized light source. The measured polarization, at electron energies from threshold to 100 eV, was found to be less than 10% for all transitions, leading to a negligible correction [10] to our cross-section measurements.

III. RESULTS

A. Optical-emission cross sections

The measured optical-emission cross sections for the 30 lines of $3p \rightarrow 1s$ transition array are listed in Table IV for an electron energy of 40 eV and a target gas pressure of 6 mTorr. For the seven transitions (see Table I) which had the possibility of contamination by an argon-ion emission line as evidenced by a sharp increase in the cross section above the ~ 35 eV threshold for excitation of the ion lines, we took measurements at 20 eV and used an uncontaminated line arising from the same upper state to extrapolate to 40 eV. For the emissions at 419.1 nm ($3p_4 \rightarrow 1s_3$, $3p_8 \rightarrow 1s_5$), we used the transition probabilities of Ref. [8] along with our measurements of other $3p_4$ and $3p_8$ emission lines to apportion the signal. In almost all cases the relative $3p \rightarrow 1s$ emission intensities agree well with the relative $3p \rightarrow 1s$ transition probabilities of Ref. [8]. The few transitions that differ by more than 20% are generally weaker lines (with optical-emission cross sections $< 10^{-20}$ cm^2).

Optical-emission cross sections for 14 of the $4p \rightarrow 1s$ transitions and five of the $5p \rightarrow 1s$ transitions are listed in Table V for an electron energy of 40 eV and a target gas pressure of 6 mTorr. Due to weak signal rates and ion-line contamination, we generally only measured one transition out of each excited state. For the four cases where we could compare transitions arising from the same upper state, three levels ($4p_5, 4p_6, 4p_{10}$) compare well with published transition probabilities [17]. The ratio of the intensities for the transitions out of the $4p_3$ level, however, differ by a factor of 2 compared to the ratio of the corresponding transition probabilities (cf. Tables III and V).

B. Cascades and pressure effects

The measured optical-emission cross sections include contributions from direct electron-impact excitation and electron-impact excitation into higher levels that radiatively decay down into the levels of interest. This indirect contribution can be corrected for by measuring the optical cross sections for the cascade transitions from the higher levels as illustrated in Eq. (5). Most of these cascades lie too far in the infrared (>3 μm) for our possible measurement, hence we can not determine direct cross sections from our data.

The only levels that are dipole allowed to decay into the $3p$, $4p$, and $5p$ levels are levels of the $3p^5ns$ and $3p^5nd$ configurations. Of these levels, of special note are those with $J=1$ which are also resonance levels whose cross section as a function of energy is generally characterized by a broad maximum around 50 eV [24]. Furthermore, these same resonance levels also exhibit resonance radiation trapping which leads to a pressure-dependent branching fraction of these resonance levels to their decay channels [25]. The radiation trapping of higher-lying cascade levels can thus lead to a pressure dependence of the $3p$, $4p$, and $5p$ optical-emission cross sections. In Fig. 1, we plot the dependence of the observed cross sections on the target gas pressure for selected $3p$ levels at two electron energies.

The relative degree of pressure dependence depends on two main factors. First, the branching fraction of the higher resonance levels into the particular level of interest, and second the comparative size of the direct excitation process. In most cases at the peak of the cross section ($\sim$20 eV), the direct cross section is much larger than the cascade contribution, hence the cross section is essentially independent of pressure. At high energies (such as 100 eV) cascades from radiation-trapped resonance levels make up a larger fraction of the signal, which result in the observed increases in the optical-emission cross sections with pressure. An excellent example of these two general patterns is seen in the emissions from the $3p_2$ level, with the 20-eV results independent of pressure, whereas the 100-eV results increase by a factor of 2 as the pressure is increased from 0.5 mTorr to 6 mTorr. Two other levels illustrate the role the branching fraction of cascade levels and the size of the direct cross section can play on the observed pressure dependence. The $3p_7$ level receives a larger amount of the emissions from higher resonance levels than do the other $3p$ levels. As a result, the cascade contribution is substantial even at low energies

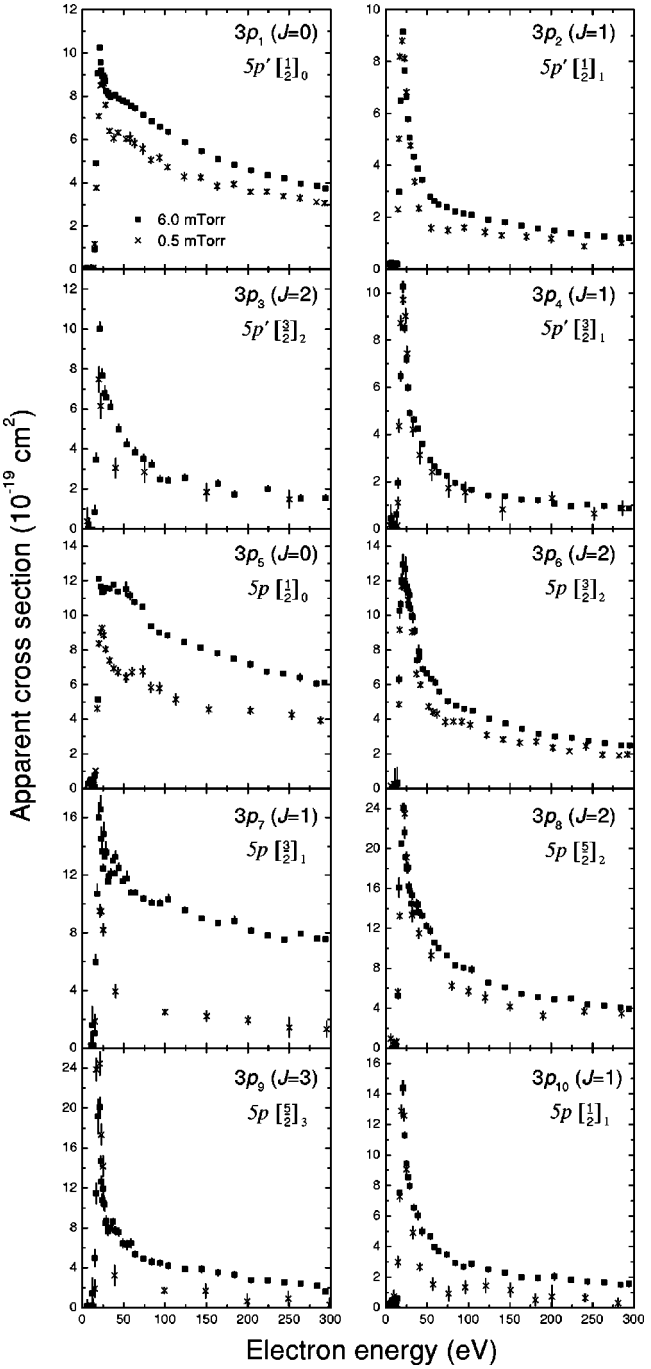

FIG. 2. Apparent cross sections for $3p$ levels. The energy dependence of Q^{app} was found by measuring the following optical-emission cross sections: 425.9 nm ($3p_1$), 418.2 nm ($3p_2$), 433.4 nm ($3p_3$), 434.5 nm ($3p_4$), 451.1 nm ($3p_5$), 415.9 nm ($3p_6$), 427.2 nm ($3p_7$), 462.8 nm ($3p_8$), 420.1 nm ($3p_9$), 425.1 nm ($3p_{10}$). Error bars are statistical only and do not include the uncertainties from the absolute calibration and transition probabilities used to convert Q^{opt} to Q^{app}.

where the direct cross section usually dominates. As the pressure is increased from 0.5 mTorr to 6 mTorr the optical-emission cross section doubles at 20 eV, and increases by a factor of 5 at 100 eV. In contrast, the $J=3$ $3p_9$ receives no cascades directly from $J=1$ resonance levels, yet still shows significant pressure dependence at 100 eV. The cause in this

case is due to an extremely small direct excitation contribution. The $3p_9$ level being a pure triplet level ($^3D_3$) has a very small direct excitation cross section from the $^1S_0$ ground state at 100 eV. Thus even a small amount of pressure-dependent cascades (from multistep cascade processes) can have a comparable magnitude to the small direct cross section.

C. Apparent cross sections

Using the procedure involving transition probabilities and atomic lifetimes outlined in Sec. II, we have converted our $3p \rightarrow 1s$ optical-emission cross sections into apparent cross sections for the $3p$ levels. The resulting values at 40 eV and both 6 mTorr and extrapolated to 0 mTorr are included in the last two rows of Table IV. Due to the added uncertainties introduced from the transition probabilities, the uncertainties in our reported apparent cross sections are $\pm 25\%$. The energy dependence of the apparent cross sections is shown in Fig. 2. To construct this figure we took the ''best'' optical-emission cross section for each $3p$ level (listed in the figure caption) and set the value at 40 eV equal to the scaled apparent cross section. To illustrate the effect of pressure-dependent cascades, we include two sets of data taken at 0.5 mTorr and 6 mTorr. While the data taken at 6 mTorr have smaller statistical error bars, they also demonstrate the increased cascade contribution to the apparent cross section evident at high electron energies.

In Sec. I we noted that the $3p \rightarrow 2s,3d$ emissions are in the infrared which makes their measurement difficult; but, we should add, not impossible. In Ref. [24], the $3p \rightarrow 2s,3d$ optical-emission cross sections were in fact measured to find the cascade contributions to the $2s$ and $3d$ apparent cross sections. In principle, we could combine these (or similar) infrared measurements with the $3p \rightarrow 1s$ measurements presented here to obtain $3p$ apparent cross sections without using transition probabilities. There are, however, a couple of problems with this approach. First, due to the low sensitivity of ir detectors it is difficult to measure all of the $3p \rightarrow 2s,3d$ emissions—particularly weak transitions above 3 μm. In Ref. [24] this problem was overcome by placing upper bounds on the sizes of the unresolvable optical-emission cross sections. For the cascade correction purposes of Ref. [24] this was not a problem as long as the upper bounds on the unmeasured cascade cross sections were much less than the $2s$ and $3d$ apparent cross sections. For the purposes of this work, however, we need to compare size of these upper bounds to the much smaller $3p$ apparent cross sections. This comparison is far less favorable. Second, the combined low sensitivity, increased thermal blackbody background, and many cross calibration steps necessary to measure absolute intensities above 3 μm lead to relatively large uncertainties ($\sim 40\%$) in those $3p \rightarrow 2s,3d$ emission cross sections that can be measured. Once again, this level of uncertainty is not a problem in a small cascade correction, but is substantial when finding the $3p$ apparent cross section. Hence, we find it more advantageous to use transition probabilities to fill in the missing transitions ($\pm 25\%$ uncertainty) than using direct infrared measurements ($\pm 40\%$ uncertainty or even higher).

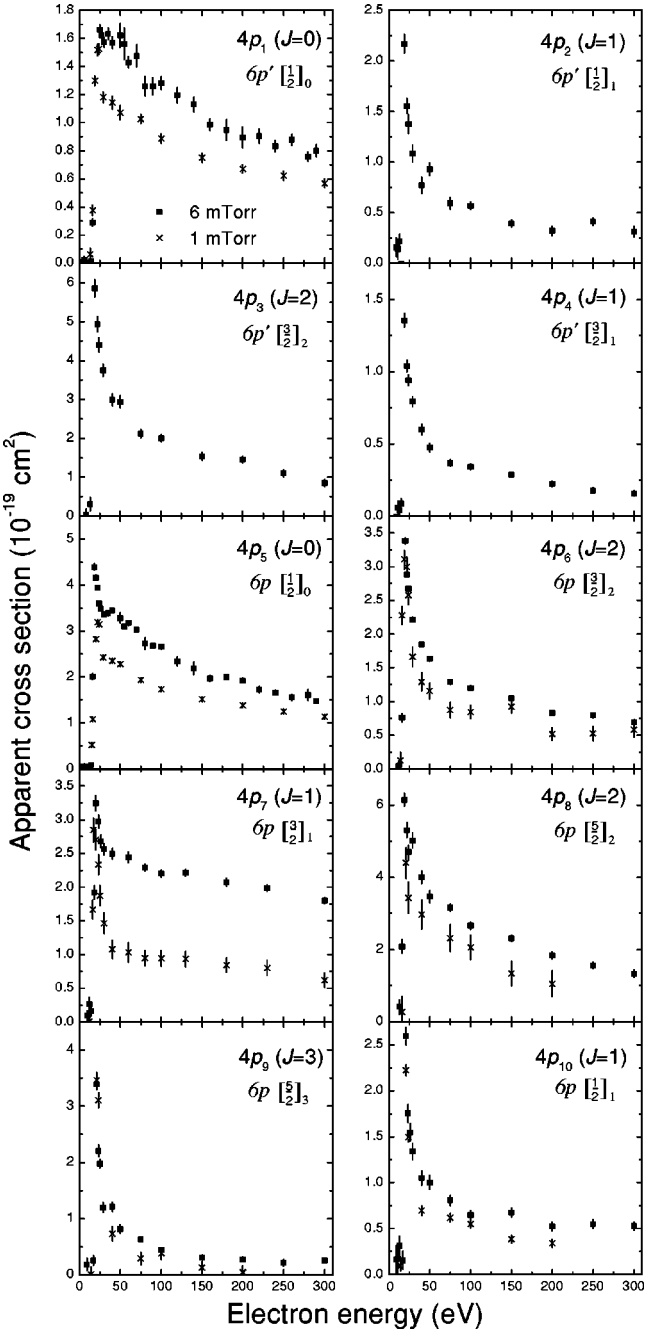

FIG. 3. Apparent cross sections for $4p$ levels. The energy dependence of Q^{app} was found by measuring the following optical-emission cross sections: 365.0 nm ($4p_1$), 339.4 nm ($4p_2$), 346.1 nm ($4p_3$), 339.3 nm ($4p_4$), 383.5 nm ($4p_5$), 355.4 nm ($4p_6$), 374.4 nm ($4p_7$), 364.3 nm ($4p_8$), 356.8 nm ($4p_9$), 389.5 nm ($4p_{10}$).

We have also converted our $4p,5p \rightarrow 1s$ optical-emission cross sections into apparent cross sections for the 12 of the 15 levels that we have reliable transition-probability values for. This was also done using Eq. (4) by limiting the summations to only those transitions we observed. The resulting values at 40 eV are included in the last column of Table V.

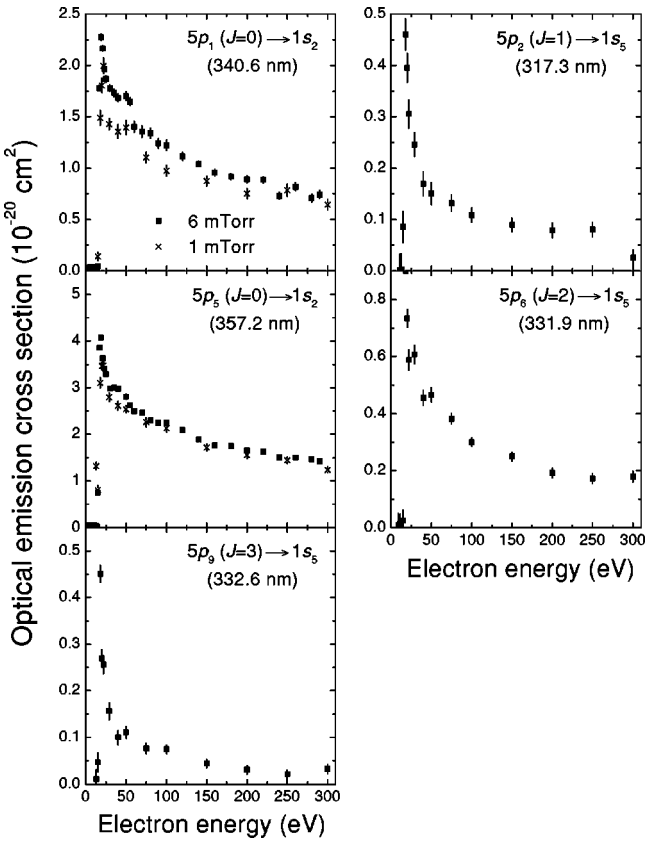

FIG. 4. Optical-emission cross sections for selected $5p$ levels. Error bars are statistical only.

The energy dependence for the levels are displayed in Fig. 3 for the $4p$ levels and Fig. 4 for the $5p$ levels.

D. Cross sections for plasma applications

In a plasma where electron-impact excitation is the major mechanism of producing excited atoms, the population of an excited level arises from both direct excitation as well as cascades from higher levels. Thus it is the *apparent* excitation cross sections that are most relevant to the analysis of optical-based plasma diagnostics, since the ''correction'' for the cascade contribution is included in the cross-section measurement, whereas the *direct* excitation cross sections (in addition to their fundamental importance in collision physics) are more relevant to comprehensive plasma modeling where the collisional and radiative transfer rates between each individual level are considered seperately.

Furthermore, for plasma diagnostic purposes, it is more convenient to work with optical-emission cross sections rather than apparent cross sections since individual transition intensities are the observed quantity. Optical-emission cross sections (at any energy) can be extracted from the apparent cross section values in Figs. 2 and 3 by using Eq. (3) along with the appropriate $3p$ (or $4p$) to $1s$ transition probabilities (i.e., Refs. [8,11,17]) and inverse lifetime values listed in Tables II and III. Two notes of caution are warranted in using this procedure. First, for many of the emission lines there are ion or atomic emission lines close by in wavelength (see Table I). For instance, above 30 eV the extremely weak $3p_1 \rightarrow 1s_4$ emission line at 398.0 nm is completely overwhelmed by emissions from an Ar^+ line at 397.9 nm. Second, as described in Sec. III B the observed optical/apparent cross sections can vary with pressure due to radiation trapping of cascading resonance levels. Except for the $3p_7$ and $4p_7$ levels (and to a lesser extent, the $3p_5$ and $4p_5$ levels), this is a small effect for electron energies near threshold; but at higher energies this pressure dependence becomes much larger.

IV. DISCUSSION

A. Comparison to previous measurements

The $3p \rightarrow 1s$ optical-emission cross sections have been measured to various degrees of completeness a number of

TABLE VI. Comparison of optical-emission cross-section values.

λ (nm)		Q^{opt} (10^{-19} cm^2) Peak energy (20–25 eV) This work[a]	Ref. [5]	Ref. [3]	Ref. [4][b]	100 eV This work[c]	Ref. [2]
425.9	$3p_1$	3.1	1.8	5.4	1.0	1.7	1.51
418.2	$3p_2$	0.88	0.80	1.25		0.17	0.08
434.5	$3p_4$	0.6	0.3			0.05	0.04
451.1	$3p_5$	1.2	0.72	0.85	0.27		
419.8	$3p_5$	3.3	1.2	1.4		0.66	1.1
415.9	$3p_6$	2.7	2.0		0.26	0.83	0.45
427.2	$3p_7$	1.7	0.8	0.89	0.26		
416.4	$3p_7$	0.96	0.7			0.07	0.08
430.0	$3p_8$	1.8	0.8	0.36	0.22		
462.8	$3p_8$	0.16		0.49		0.04	0.04
420.1	$3p_9$	2.7	2.1	6.74		0.15	0.20
470.2	$3p_{10}$	0.37	0.25			0.03	0.04

[a]6 mTorr values.

[b]Taken with a pulsed electron beam, to reduce cascade.

[c]0.5-mTorr values.

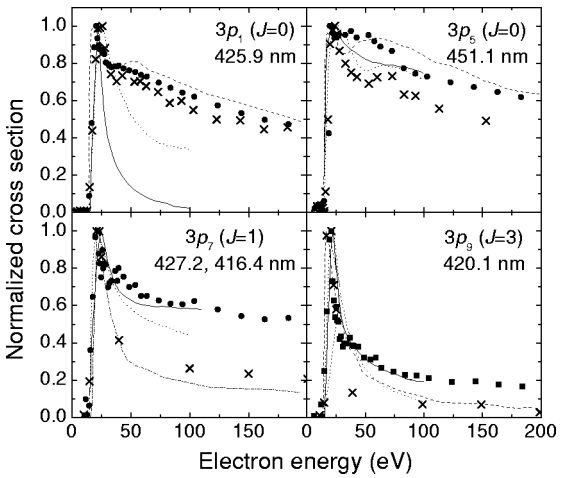

FIG. 5. Comparison of normalized cross-section shapes for selected levels. This work: 0.5-mTorr values (×), 6-mTorr values (●); Fischer [3] (solid line); Feltsan and Zapesochny [5] (dotted line); Ballou *et al.* [26] (dashed line); and Tsurubuchi *et al.* [2] (dot-dashed line).

times in the past. Fischer measured 15 of the $3p \rightarrow 1s$ transitions and found the energy dependence of the cross sections from 0 to 100 eV [3]. His relative results (obtained at 18 mTorr) were placed on an absolute scale by cross calibration to the known 435.8-nm Hg optical-emission cross section. Feltsan and Zapesochny measured 17 of the $3p \rightarrow 1s$ optical-emission cross sections from onset to 100 eV at gas pressures between 0.7 and 3 mTorr [5]. Bogdanova and Yurgenson used a time resolved measurement technique with a pulsed electron beam to measure seven $3p \rightarrow 1s$ optical-emission cross sections at 25 eV [4]. While their measurements were done at a high gas pressure (10 mTorr) where pressure-dependent cascades can be large, time resolved measurements were used to reduce the amount of cascades. These authors also used transition probabilities to convert their optical-emission cross sections into apparent cross sections. Finally, Tsurubuchi *et al.* have recently measured 12 of the 30 $3p \rightarrow 1s$ optical-emission cross sections for the purposes of correcting their $1s$ apparent cross sections for cascades [2]. Their measurements were done at very low pressure, but they only report values at 100 eV except for a full $3p_7$ excitation function.

A comparison of the present work with these earlier measurements is found in Table VI. Our values at the peak energy are generally larger than those of Ref. [5], and smaller than those of Ref. [3]. Since the gas pressure at which we obtained our results is also intermediate between that used by Refs. [3,5], much of the variation is due to differing contributions of radiation-trapped cascading levels. For those cases where multiple transitions are measured out of a common upper state, our intensity ratios agree slightly better with transition probabilities than do the results of the other experiments. In almost all cases we agree well within error bars with the 100-eV low-pressure results of Ref. [2]. In contrast, our results are much larger than the cascade-reduced measurements of Ref. [4]. This could argue for either a substantial cascade contribution ($>75\%$), or some problem with the pulsed measurements. The best approach to resolving this question would be to directly measure the cascading transitions, however these generally have long wavelengths ($\gg 3$ μm) making their measurement very difficult. However, for the $3p_1$ level we can possibly resolve this issue without directly measuring the cascades. The only dipole-allowed cascading transitions into the $J=0$ $3p_1$ level are from $J=1$ resonance levels. Since these levels are subject to radiation trapping, if cascades make up a large fraction of the $3p_1$ apparent cross section then the 425.9-nm $3p_1 \rightarrow 1s_2$ emission cross section should exhibit severe pressure dependence. However, as shown in Fig. 1, at 20 eV the $3p_1$ level has a rather weak pressure dependence which argues against a large cascade contribution.

The energy dependence of the cross sections measured in this work is in excellent agreement with the earlier relative measurements of Ballou *et al.* [26], and reasonable agreement with the excitation functions of Refs. [3,5] with the notable exception of the $3p_1$ level as shown in Fig. 5. The $3p_7$ level is also an interesting case due to the strong pressure dependence observed in this level. Our 0.5-mTorr data closely match the sharply peaked data taken at low pressures by Tsurubuchi *et al.* [2], whereas our 6-mTorr data are similar to the broad curves measured at high pressures by Fischer [3] and Feltsan and Zapesochny [5]. The agreement between experiments for the remaining levels not shown in Fig. 5 is similar to that shown for the $3p_9$, with better than $\pm 25\%$ agreement at 100 eV.

B. Relation to other rare-gas atoms

Systematic measurements of electron-impact excitation cross sections in recent years have provided a global understanding of the excitation process of the rare-gas atoms. For the Ne$\cdots$Xe series the ground states are described by $np^6\,{}^1S_0$ where $n=2,3,4,5$ for Ne,Ar,Kr,Xe, respectively. The next two configurations $np^5(n+1)s$ and $np^5(n+1)p$ are of special interest since they are responsible for some of the strongest emissions. Electron excitation into the ten levels of the $np^5(n+1)p$ configuration ($2p$ in Paschen's notation) for all atoms have been studied in detail [1,27–29]. In this section we discuss the new cross sections for Ar($3p^5 5p$) and Ar($3p^5 6p$) in the context of the systematic behaviors of the rare-gas series.

We should first point out that the $3p^5 5p$ and $3p^5 6p$ data reported here are the apparent excitation cross sections which have not been corrected for cascades. Nevertheless, for discussing the general trends we will use the apparent cross sections in lieu of the direct excitation cross-sections, since in general the percentage cascade tends to decrease for the higher levels in the nonresonant series [30,31].

Our first observation is the magnitude of the cross sections as related to the parity of the total angular momentum J. Within the $np^5(n+1)p$ configuration the levels with even values of J have larger cross sections than the odd-J levels for all four atoms [1,27–29]. We see that our new data for the Ar($3p^5 5p$) and Ar($3p^5 6p$) cross sections indeed conform to this parity relation as well. The variation of the cross section with J has been explained qualitatively by using a

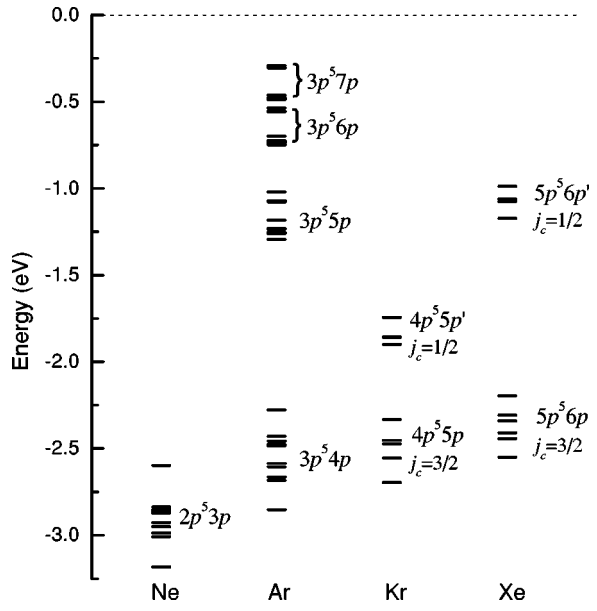

FIG. 6. Energy level spacing for $np^5n'p$ configurations of the rare gases. The energy levels are measured from the ionization limit which is taken as $E=0$.

multipole field picture, and by a group-theoretical analysis of the coupling between the initial and final states of the inelastic collision on a more quantitative basis [32,33].

The $3p^55p$ and $3p^56p$ cross sections for Ar also provide a linkage between the cross-section pattern observed for Ne and Ar and the very different pattern for Kr and Xe. To see this let us first discuss the $np^5(n+1)p$ configuration of the rare-gas atoms. We denote the orbital and spin angular momentum of the np^5 core as l_c and s_c, respectively, and use l_0 and s_0 for the corresponding quantities of the "outer" electron $(n+1)p$. The coupling of these four angular-momentum vectors are quite complicated and in general do not conform to any one of the simplest coupling schemes such as the LS, jj, and jK types [34]. For Xe the spin-orbit coupling of the core (1.3-eV splitting) dominates the couplings of the other angular momenta so that from $l_c=1$ and $s_c=1/2$ we first construct $j_c=1/2$ and 3/2. We then couple $j_c=1/2$ with $l_0=1$, $s_0=1/2$ resulting in $J=0,1,1,2$; and likewise obtain $J=0,1,1,2,2,3$ using $j_c=3/2$. We refer to this as $j_c(l_0s_0)J$ coupling since we do not specify whether j_c first couples with l_0 to form the intermediate vector K (jK coupling) or l_0 and s_0 first couple together to form j_0 (jj coupling). The ten energy levels of the Xe$(5p^56p)$ configuration indeed segregate into a lower group of six ($j_c=3/2$) and an upper group of four ($j_c=1/2$) as shown in the fourth column of Fig. 6. Interestingly, this two-tier pattern is also evident in the electron-impact excitation cross sections listed in Table VII in which we find, in the case of Xe$(5p^56p)$, the levels in the lower group to have larger cross sections than those in the upper group especially if we compare only levels of the same J parity. The ionization energies of the two groups (1.1 and 2.4 eV) differ by a factor of 2, which means that the upper-group levels have much more extended wave functions compared to members of the lower group and are therefore less likely to be excited from the ground state which has a much more compact wave function. The same analysis applies to Kr. Although Kr has a smaller core spin-orbit coupling (0.67 eV) than Xe, we see in Fig. 6 and Table VII a similar, though less distinct, two-tier separation in both the energy levels and cross sections within the Kr$(4p^55p)$ configuration.

On the opposite extreme is Ne for which the spin-orbit splitting of the $2p^5$ core is 0.097 eV, much smaller than the Coulomb interaction of the outer electron $(3p)$ with the $2p^5$ core. The $j_c(l_0s_0)J$ coupling is not a good approximation and no two-tier pattern is seen in Fig. 6 and Table VII for the energy levels and cross sections for Ne$(2p^53p)$. In contrast to Kr and Xe where the upper four levels have smaller cross

TABLE VII. Comparison of cross sections for rare-gas atoms at 75 eV. Values for $np^5(n+1)p$ configurations of Ne, Ar, Kr, and Xe are direct cross sections, values for Ar$(3p^5np,\ n=5,6,7)$ configurations are apparent cross sections at 0.5 mTorr (which include some cascade contribution). To maintain the same set of labels for all the rare gases, we designate the levels using Racah notation (which is a labeling scheme essentially based on jK coupling).

			Cross section (10^{-19} cm^2)						
	J	Racah designation	Xe$(5p^56p)$ Ref. [29]	Kr$(4p^55p)$ Ref. [28]	Ne$(2p^53p)$ Ref. [27]	Ar$(3p^54p)$ Ref. [1]	Ar$(3p^55p)$ This work	Ar$(3p^56p)$ This work	Ar$(3p^57p)$ This work
$j_c=\frac{1}{2}$	0	$p'[\frac{1}{2}]_0$	22	20	16	30	5.3	1.0	0.56
	1	$p'[\frac{1}{2}]_1$	2.4	7.2	3.2	6.9	1.5	0.59	
	1	$p'[\frac{3}{2}]_1$	1.5	7.0	2.4	7.2	1.7	0.37	
	2	$p'[\frac{3}{2}]_2$	19	23	9.9	12	2.9	1.8	
$j_c=\frac{3}{2}$	0	$p[\frac{1}{2}]_0$	94	41	2.4	13	6.3	1.9	1.2
	1	$p[\frac{1}{2}]_1$	50	8.5	2.8	7.3	1.3	0.62	
	1	$p[\frac{3}{2}]_1$	32	29	3.5	11	3.2	0.93	
	2	$p[\frac{3}{2}]_2$	38	26	11	16	3.9	0.87	
	2	$p[\frac{5}{2}]_2$	50	44	6.5	23	6.9	2.3	
	3	$p[\frac{5}{2}]_3$	3.1	15	3.9	4.3	2.5	0.29	

sections than the lower six within the $np^5(n+1)p$ configuration, it is the uppermost level that has the largest cross section in Ne$(2p^5 3p)$. Ar has a somewhat larger spin orbit of the core (0.18 eV) than Ne, but still much smaller than the Kr value. This is reflected by the similarity of Ar$(3p^5 4p)$ to Ne$(2p^5 3p)$ in the general pattern of both energy levels and cross sections (Fig. 6 and Table VII).

The variations of the cross sections with the angular-momentum vector coupling can be delineated more quantitatively by considering the two $J=0$ levels of the $np^5(n+1)p$ configuration in greater detail. Note in Table VII the dominance of the upper $J=0$ level over the lower $J=0$ level in the case of Ne cross sections whereas the trend is reversed for Xe and Kr. Let us start with the limit of zero spin-orbit coupling (close to the Ne extreme) for the $(np^5)(n'p)$ configuration and refer to this as the unperturbed system. The ''unperturbed energies'' for the six terms in the LS representation (^1S, ^3S, ^1P, ^3P, ^1D, ^3D) are expressible in terms of the Slater-Condon parameters involving the np and $n'p$ electrons with ^1S term having the highest energy [35]. Introduction of a small or moderate spin-orbit coupling as a perturbation splits the ^3P term into an inverted triplet ($J=0,1,2$) and allows the top member $^3P_0$ to interact with the only other $J=0$, $^1S_0$. This results in two levels described by

$$|a\rangle = \alpha|^1S_0\rangle + \beta|^3P_0\rangle,$$

$$|b\rangle = \beta|^1S_0\rangle - \alpha|^3P_0\rangle. \quad (6)$$

For the case of weak spin-orbit interactions, the $^1S_0$ term is well above the $^3P_0$ term, so that with only a small admixture in Eq. (6) the upper level is mostly singlet and the lower level is mostly triplet. Since the ground state np^6 is purely singlet, excitation into the upper $J=0$ level has a larger cross section than into the lower one. For a more quantitative illustration consider the Ne$(2p^5 3p)$ configuration. Using the Slater-Condon parameters of Ref. [34] we have the unperturbed energy spacing between $^1S_0$ and $^3P_0$ as 2100 cm^{-1} which is indeed much larger than the $2p^5$ spin-orbit coupling parameter $\zeta = 333$ cm^{-1} [34], leading to an estimate of the admixture coefficient $\beta \sim 0.16$ and $\alpha = \sqrt{1-\beta^2} \sim 0.98$. A more elaborate calculation based upon the method of Cowan and Andrew [34] yields $\alpha = 0.98$ and $\beta = 0.18$. Thus the upper Ne $J=0$ level has only a 3% triplet character. For the Ar$(3p^5 4p)$ configuration a similar calculation gives $\alpha = 0.89$ and $\beta = 0.45$ because the spin-orbit coupling, is much stronger. Thus, the disparity between the two $J=0$ levels decreases with an increasing amount of admixture due to the spin-orbit interaction. Further increase of the spin-orbit splitting eventually pushes the $|^3P_0\rangle$ energy above the $|^1S_0\rangle$. When their mixing is taken into account as in Eq. (6), the lower $J=0$ level now has a larger singlet component, and therefore larger cross-section, than the upper one. Indeed we find the upper-vs-lower cross-section ratio to be 6.7 for Ne and 2.3 for Ar, but 0.5 for Kr and 0.23 for Xe.

The higher configurations $3p^5 n'p$ of Ar studied in this paper now provide another way of examining the differences in going from intermediate coupling (Ne,Ar) to $j_c(l_0 s_0)J$ coupling (Kr,Xe). Let us compare the $3p^5 4p$ and $3p^5 5p$ configurations. They share the same $3p^5$-core spin-orbit splitting, but the interaction of the core with the outer electron is smaller for the $3p^5 5p$ since the outer $5p$ electron is further away from the core. Thus for higher configurations the core-spin-orbit interaction becomes more important relative to the interaction of the core with the outer electron shifting the coupling toward the $j_c(l_0 s_0)J$ scheme. In reference to Fig. 6 the energy levels of the Ar$(3p^5 6p)$ configuration clearly segregate into two groups, but this pattern is less obvious for Ar$(3p^5 5p)$. Correspondingly the Ar$(3p^5 6p)$ cross sections also fall into the two-tier structure with the lower group having cross sections on average 35% larger than the upper group, whereas the same division of cross sections is not recognizable for the Ar$(3p^5 5p)$ configuration. In the preceding paragraph we discuss the cross-section ratio of the upper $J=0$ vs the lower $J=0$ level which is 2.3 for the Ar$(3p^5 4p)$ configuration and 0.50 for Kr$(4p^5 5p)$. For the Ar$(3p^5 5p)$, Ar$(3p^5 6p)$, and Ar$(3p^5 7p)$ configurations, this ratio is 0.83, 0.53, and 0.47, respectively, mirroring the transition from intermediate coupling of Ne$(2p^5 3p)$ and Ar$(3p^5 4p)$ to the $j_c(l_0 s_0)J$ coupling of Kr and Xe.

ACKNOWLEDGMENTS

The authors wish to thank Professor Donald W. Setser for discussions concerning the lifetime measurements. This work was supported by the Air Force Office of Scientific Research.

[1] J.E. Chilton, J.B. Boffard, R.S. Schappe, and C.C. Lin, Phys. Rev. A **57**, 267 (1998).
[2] S. Tsurubuchi, T. Miyazaki, and K. Motohashi, J. Phys. B **29**, 1785 (1996).
[3] O. Fischer, Z. Phys. **86**, 646 (1933).
[4] I.P. Bogdanova and S.V. Yurgenson, Opt. Spektrosk. **68**, 1246 (1990) [Opt. Spectrosc. **68**, 730 (1990)].
[5] P.V. Feltsan and I.P. Zapesochny, Ukr. Fiz. Zh. (Russ. Ed.) **12**, 633 (1967).
[6] G. Crolly and H. Oechsner, Eur. Phys. J. A **15**, 49 (2001).
[7] A. Bogaerts and R. Gijbels, J. Anal. At. Spectrom. **16**, 239 (2001).
[8] W.L. Wiese, J.W. Brault, K. Danzmann, V. Helbig, and M. Kock, Phys. Rev. A **39**, 2461 (1989).
[9] D.W. Jones and W.L. Wiese, Phys. Rev. A **39**, 110 (1989).
[10] A.R. Filippelli, C.C. Lin, L.W. Anderson, and J.W. McConkey, Adv. At., Mol., Opt. Phys. **33**, 1 (1994).
[11] J.P. Knauer and M. Kock, J. Quant. Spectrosc. Radiat. Transf. **51**, 723 (1994).
[12] J.Z. Klose, J. Opt. Soc. Am. **58**, 1509 (1968).
[13] G. Inoue, D.W. Setser, and N. Sadeghi, J. Chem. Phys. **76**, 977 (1982).
[14] M.J.G. Borge and J. Campos, Physica C **119**, 359 (1983).
[15] Z. Stryla, H. Pobee, W. Schade, and V. Helbig, Phys. Rev. A

41, 512 (1990), and references therein.
[16] A. Hirabayashi, S. Okuda, Y. Nambu, and T. Fujimoto, Phys. Rev. A **35**, 639 (1987), and references therein.
[17] NIST Atomic Spectra Database, URL http://physics.nist.gov/asd
[18] B.S. Malone and W.H. Corcoran, J. Quant. Spectrosc. Radiat. Transf. **6**, 443 (1966).
[19] B. Zurro, J. Campos, and C.S. del Rio, Phys. Lett. **43A**, 527 (1973).
[20] J.A. Aguilera, F. Blanco, J. Campos, and M. Ortiz, Phys. Rev. A **45**, 2753 (1992).
[21] I.N. Bagaeva and M.P. Chaika, Vestn. Leningr. Univ., Ser. 4: Fiz., Khim. **4**, 80 (1988).
[22] N.V. Afanaseva and P.F. Gruzdev, Opt. Spektrosk. **38**, 794 (1975) [Opt. Spectrosc. **38**, 450 (1975)].
[23] B. Van Zyl, G.H. Dunn, G. Chamberlain, and D.W.O. Heddle, Phys. Rev. A **22**, 1916 (1980).
[24] J.E. Chilton and C.C. Lin, Phys. Rev. A **60**, 3712 (1999).
[25] M.D. Stewart, J.E. Chilton, J.B. Boffard, and C.C. Lin, Phys. Rev. A **65**, 032704 (2002).
[26] J.K. Ballou, C.C. Lin, and F.E. Fajen, Phys. Rev. A **8**, 1797 (1973).
[27] J.E. Chilton, M.D. Stewart, and C.C. Lin, Phys. Rev. A **61**, 052708 (2000).
[28] J.E. Chilton, M.D. Stewart, and C.C. Lin, Phys. Rev. A **62**, 032714 (2000).
[29] J.T. Fons and C.C. Lin, Phys. Rev. A **58**, 4603 (1998).
[30] J.O. Phelps, J.E. Solomon, D.F. Korff, C.C. Lin, and E.T.P. Lee, Phys. Rev. A **20**, 1418 (1979).
[31] J.O. Phelps and C.C. Lin, Phys. Rev. A **24**, 1299 (1981).
[32] F.A. Sharpton, R.M. St. John, C.C. Lin, and F.E. Fajen, Phys. Rev. A **2**, 1305 (1970).
[33] J.B. Boffard, G.A. Piech, M.F. Gehrke, L.W. Anderson, and C.C. Lin, Phys. Rev. A **59**, 2749 (1999).
[34] R.D. Cowan and K.L. Andrew, J. Opt. Soc. Am. **55**, 502 (1965).
[35] E.U. Condon and G.H. Shortley, *The Theory of Atomic Spectra* (Cambridge University Press, London, 1963).